NeuroImage 260 (2022) 119455

Contents lists available at ScienceDirect

NeuroImage

journal homepage: www.elsevier.com/locate/neuroimage

Structural connections between the noradrenergic and cholinergic system shape the dynamics of functional brain networks

N.L. Taylor[a], A. D'Souza[a,b], B.R. Munn[a], J. Lv[a,c], L. Zaborszky[d], E.J. Müller[a], G. Wainstein[a], F. Calamante[a,c,e], J.M. Shine[a,*]

[a] Brain and Mind Centre, The University of Sydney, Sydney, Australia
[b] Sydney School of Medicine, Central Clinical School, The University of Sydney, Australia
[c] School of Biomedical Engineering, The University of Sydney, Sydney, Australia
[d] School of Arts and Sciences, Rutgers University, New Jersey, USA
[e] Sydney Imaging, The University of Sydney, Sydney, Australia

ARTICLE INFO

Keywords:
Locus coeruleus
Basal nucleus of Meynert
Diffusion MRI
Attractor landscape
Neuromodulation

ABSTRACT

Complex cognitive abilities are thought to arise from the ability of the brain to adaptively reconfigure its internal network structure as a function of task demands. Recent work has suggested that this inherent flexibility may in part be conferred by the widespread projections of the ascending arousal systems. While the different components of the ascending arousal system are often studied in isolation, there are anatomical connections between neuromodulatory hubs that we hypothesise are crucial for mediating key features of adaptive network dynamics, such as the balance between integration and segregation. To test this hypothesis, we estimated the strength of structural connectivity between key hubs of the noradrenergic and cholinergic arousal systems (the locus coeruleus [LC] and nucleus basalis of Meynert [nbM], respectively). We then asked whether the strength of structural LC and nbM inter-connectivity was related to individual differences in the emergent, dynamical signatures of functional integration measured from resting state fMRI data, such as network and attractor topography. We observed a significant positive relationship between the strength of white-matter connections between the LC and nbM and the extent of network-level integration following BOLD signal peaks in LC relative to nbM activity. In addition, individuals with denser white-matter streamlines interconnecting neuromodulatory hubs also demonstrated a heightened ability to shift to novel brain states. These results suggest that individuals with stronger structural connectivity between the noradrenergic and cholinergic systems have a greater capacity to mediate the flexible network dynamics required to support complex, adaptive behaviour. Furthermore, our results highlight the underlying static features of the neuromodulatory hubs can impose some constraints on the dynamic features of the brain.

1. Introduction

The human brain contains exquisite structural complexity – billions of neurons share trillions of connections that integrate and coordinate their electrophysiological activity, and this has only recently become non-invasively interrogable via advances in diffusion weighted imaging (Catani & Thiebautdeschotten, 2008; Schilling et al., 2021). Despite these advances, precisely how the many and varied functions of the human brain emerge from the complex constraints of the structural connectome remains poorly understood. For instance, while there is substantial evidence for a relationship between structural and functional connectivity (Mišić et al., 2016; Seguin et al., 2020; Shen et al., 2015; Suárez et al., 2020; Zimmermann et al., 2016), axonal connections between regions cannot be solely used to render inferences of brain function (Honey et al., 2009; Uddin, 2013). This suggests that, whilst the structure of the brain does in some way specify underlying functional capacities, there are critical features of neuroanatomy less amenable to identification via traditional approaches that are required to fully specify the rules governing complex, adaptive brain function.

Recent research has suggested that complex cognitive abilities are conferred by the brains' capacity to adaptively reconfigure its network structure in response to varying stimuli and task contexts (Cohen & D'Esposito, 2016; Shine et al., 2016). Graph theoretical analysis has provided a means for measuring the dynamic complexity of the brain through systems level features of network activity within a robust mathematical framework (Rubinov & Sporns, 2010). These shifts in network topology fall along an axis defined by two extremes: segregated states in which regions are strongly connected to other regions within tight-knit 'communities' and weakly connected outside these communities, and integrated states that refer to strong functional connections between

* Corresponding author.
E-mail address: mac.shine@sydney.edu.au (J.M. Shine).

https://doi.org/10.1016/j.neuroimage.2022.119455.
Received 30 March 2022; Received in revised form 3 July 2022; Accepted 5 July 2022
Available online 7 July 2022.

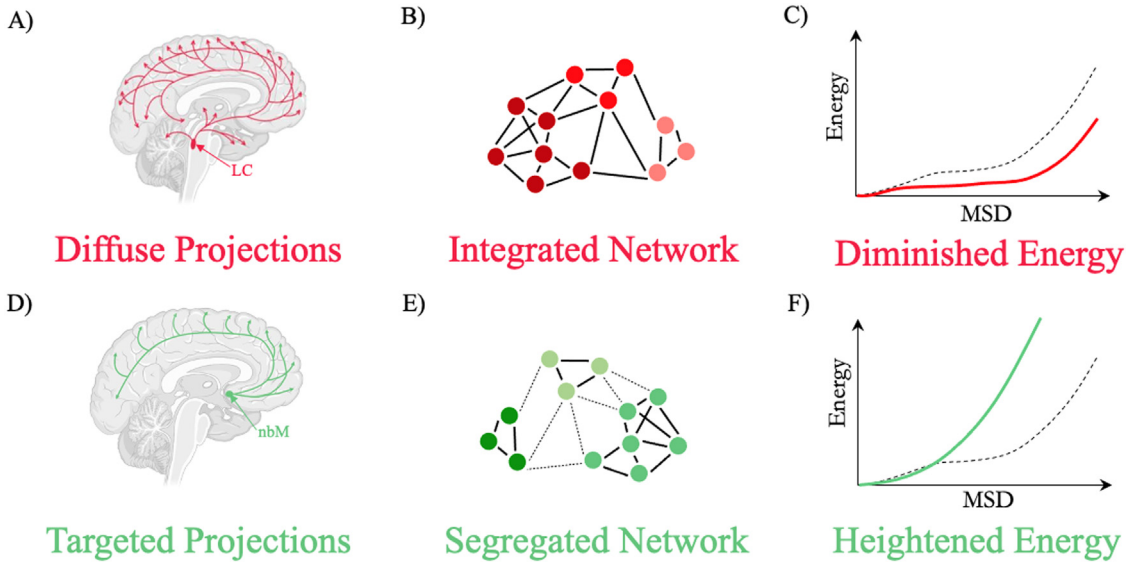

Fig. 1. The noradrenergic and cholinergic systems facilitate complex brain network topological shifts. A) The diffuse noradrenergic projections of the LC (red). B) Graphical representation of integrated network hubs. C) Adrenergic activity 'flattens' the attractor landscapes of the brain (dashed line) by decreasing the energy of all possible brain-states (red) D) The targeted projections of the cholinergic nbM (green). E) Graphical representation of segregated network hubs. F) Cholinergic activity quenches changes to brain-state by 'deepening-wells' of the attractor landscape (green).

regions of different communities (Sporns, 2013). There is now ample evidence from a range of studies that demonstrates brain network reconfiguration as a function of cognitive performance (Bassett et al., 2011, 2015; Braun et al., 2015; Fransson et al., 2018; Hearne et al., 2017; Ito et al., 2020; Mohr et al., 2016; Patil et al., 2021; Shine & Poldrack, 2018). Hence, the flexibility of the brain to shift between segregated and integrated states is inherently important in understanding brain function, but the underlying neural mechanism that gives rise to the flexibility in brain states is poorly understood.

Whilst there are numerous structures in the brain that shape intrinsic cortical variability, the components of the neuromodulatory systems are a primary candidate for enabling the brain to flexibly shift network topology (Mei et al., 2022; Müller et al., 2020; Munn et al., 2021; Shine, Aburn, et al., 2018; Shine et al., 2016, 2019, 2021a; Wainstein et al., 2021). The neuromodulatory systems consists of a range of autonomous nuclei across the brainstem and forebrain that send diverse anatomical projections throughout the brain, wherein they release neurotransmitters that engage second-messenger cascades within target neurons that alter the receptivity and/or excitability of neurons (Marder, 2012; Shine, 2019). The influence of these regions ultimately leads to large-scale effects on macroscopic neural dynamics (Brown et al., 2011; Shine et al., 2021a) that are known to facilitate novel dynamical regimes (Aston-Jones & Cohen, 2005; McGinley et al., 2015; Wainstein et al., 2022).. In support of this mechanism, recent modelling work established that increasing diffuse cortical coupling across the brain – a feature that mimics aspects of the ascending arousal system – resulted in multi-stable dynamics that maximise the temporal flexibility of brain states (Müller et al., 2020). Despite their substantial impact on the brain, their small size and strong interconnections make the hubs of the neuromodulatory system inherently challenging to study with traditional neuroimaging approaches (Alcedo & Prahlad, 2020). For these reasons, the neuromodulatory systems are commonly studied in isolation, such that there is little understanding of the interactions between different neuromodulatory systems and whether different systems will work antagonistically or synergistically to facilitate brain function.

Whilst there are multiple different neuromodulatory systems in the brain, the noradrenergic and cholinergic systems are prime candidates for influencing broad-scale neural dynamics and shifting network topology (Shine, 2019) (Fig. 1B, E). The primary cortically-projecting hubs of these systems – the noradrenergic locus coeruleus (LC) (Carter et al., 2010) and cholinergic nucleus basalis of Meynert (nbM) (Lee & Dan, 2012) – are capable of altering oscillatory activity across the brain: typically by decreasing low-frequency synchronous brain activity, whilst concurrently increasing high-frequency brain activity (Castro-Alamancos & Gulati, 2014; Lin et al., 2015; Mena-Segovia et al., 2008). This can ultimately change the timescale of neural influences on the brain network (Shine, 2019). Interestingly, despite similar mechanisms of action, the noradrenergic and cholinergic systems are associated with distinct cognitive signatures: the cholinergic system has been implicated in attentional selection, enhanced cue detection, memory encoding and cognitive specificity (Hasselmo & Sarter, 2011; Noudoost & Moore, 2011), whereas the noradrenergic system is involved in coordinating arousal (Samuels & Szabadi, 2008) optimizing the balance between task-performance (Aston-Jones & Cohen, 2005) salience detection (Sara & Bouret, 2012) and exploratory behaviours (Sara & Bouret, 2012).

The noradrenergic and cholinergic systems also have different projection patterns in the brain. While the noradrenergic LC sends vast projections around the entire cortex (Kim et al., 2016; Samuels & Szabadi, 2008) (Fig. 1A), the cholinergic nbM instead projects in a much more targeted manner to disparate sites around the cerebral cortex (Kim et al., 2016; Zaborszky et al., 2015) (Fig. 1D). Based on these features, we recently proposed that recruitment of the noradrenergic system would shift the networks of the brain into a state of increased network integration (Shine, Aburn, et al., 2018; Shine, van den Brink, et al., 2018), whereas the cholinergic system has been implicated in a relative segregation of network topology (Zaborszky et al., 2015). In previous work, we have observed evidence for these network effects in 7T resting state fMRI data (Munn et al., 2021). In addition, the LC is known to send projections to the nbM that ultimately excite the cholinergic nucleus, however the same is not true for the nbM, which can only affect LC indirectly through shared targets (Schwarz & Luo, 2015; Zaborszky et al., 1993, 2015; Zaborszky & Gombkoto, 2017). This "one-way" connection implies a precise topological relationship between the LC and nbM that likely provides important constraints over how these two hubs impact evolving brain dynamics.

In addition to altering network topology, the noradrenergic and cholinergic systems can also impact brain state dynamics over time,

in a manner that is well-captured by the dynamical systems theory concept of an attractor landscape (John et al., 2022). Briefly, this approach creates a low-dimensional topological representation of changes in systems-level neural dynamics where the probability of the occurrence of a brain state (instantaneous neural activity) can be related to a statistical 'energy' required to reach that state – for instance, a common (rare) brain state would be associated with a low (high) energy. Just like a contour winds its way across the land, individual trajectories across the state space represent unique individual cognitive states. Using this framework, we found that following phasic bursts of the LC, the attractor landscape was flattened (relative to resting dynamics) – the brain entered into a state that lowered previously high-energy transitions (Fig. 1C) (Munn et al., 2021). In contrast, phasic bursts of the nbM deepened the local wells of the attractor landscape (Fig. 1F), suggesting that the brain was confined into a particular state (Munn et al., 2021). Despite these links, to date little research has established the relationship between these effects and individual differences in white matter connections strength between the noradrenergic and cholinergic hubs, and its role in governing dynamic brain topology. Interestingly, cholinergic neurons in the basal forebrain receive extensive, excitatory (i.e., G*q*-mediated) synaptic projections from the LC, but do not send projections back (Hajszán & Zaborszky, 2002; Smiley et al., 1999; Zaborszky et al., 1993), implying a dependent topological relationship whose functional implications remain poorly understood.

Here, we investigated the relation of structural connections between hubs of the noradrenergic and cholinergic systems and emergent properties of dynamic functional network topology and energy/attractor landscape topography. Specifically, we used an advanced quantitative fibre tractography analysis of high-resolution diffusion weighted imaging from the Human Connectome Project to estimate the strength of white matter connections between projection hubs of the cholinergic and noradrenergic arousal systems. We then used time-varying functional connectivity, network topology, and energy/attractor landscape analyses to characterise the relationship between flexible network architecture and the strength of structural connectivity between the LC and nbM. Through this approach, we highlight clear relationships between structure and function that travel through neuromodulatory intermediates to shape and constrain flexible network-level signatures of adaptive brain function.

2. Methods

2.1. MRI acquisition

We used the multi-modal neuroimaging data available from the Human Connectome Project (HCP) (Van Essen et al., 2013), which was acquired using a 3T Siemens 'Connectom' Skyra scanner and included anatomical T1-weighted imaging, structural diffusion MRI, and functional MRI data. Due to the computational requirements involved in performing rigorous advanced fibre tractography, we specifically considered 50 subjects (Age range: 22-35, 29 females) from the WU-Minn HC (Van Essen et al., 2013) as a balance between computational demands and a suitable number of subjects to characterise group behaviour. The high resolution T1-weighted data were acquired with 0.7 mm isotropic resolution, TR/TE = 2400/2.14 ms, and flip angle = 8°. The diffusion MRI protocol consisted of three diffusion-weighted shells (b-values: 1000, 2000 and 3000 s/mm^2, with 90 diffusion-weighting directions in each shell) and 18 reference volumes (b = 0 s/mm^2). Each diffusion-weighted image was acquired twice, with opposite phase-encoded direction to correct for image distortion (Andersson et al., 2003). The diffusion MRI data was acquired with 1.25 mm isotropic resolution, TR/TE = 5520/89.5 ms, and flip angle = 78°. For more details about the acquisition protocol, please refer to Van Essen et al., 2013. For each subject, 14mins of resting state fMRI data were acquired using multiband gradient-echo imaging (TR = 720ms, echo time = 33.1ms, multiband factor = 8, flip angle = 52°, field of view = 208 × 180mm, matrix = 108 × 109, 2mm isotropic voxels with 72 slices, alternate phase encoding LR/RL) (Van Essen et al., 2013).

2.2. Diffusion MRI analysis

2.2.1. Segmentation of the regions of interest

LC segmentations were obtained from Ye et al., 2021; this probabilistic map was converted to a binary mask using a threshold of 10% and the binarised LC segmentation was transformed to each participant's subject-specific T1-weighted image using ANTS (Avants et al., 2011; Tustison & Avants, 2013). A binary nbM mask was obtained from (Zaborszky et al., 2008). This mask was also transformed into the participant's T1-weighted image using ANTS (Avants et al., 2011; Tustison & Avants, 2013). All subsequent analyses were conducted in individual subject-space.

2.2.2. Diffusion MRI pre-processing and tractography

The minimally processed HCP diffusion datasets (which included correction for motion, susceptibility distortions, gradient nonlinearity and eddy currents) (Andersson & Sotiropoulos, 2015, 2016; Sotiropoulos et al., 2013) were subject to additional image processing, which included bias-field correction (Tustison et al., 2010) as well as multi-shell multi-tissue constrained spherical deconvolution to generate the fibre orientation distribution (FOD) in each voxel (Jeurissen et al., 2014; Tournier et al., 2004, 2007). These steps were implemented in accordance with previous work (Civier et al., 2019) and were performed using the *MRtrix* software package (http://www.mrtrix.org, (Tournier et al., 2012, 2019)).

The T1-weighted images were used to generate a so-called 'five-tissue-type' (5TT) image (R. E. Smith et al., 2012) using FSL (Patenaude et al., 2011; S. M. Smith, 2002; S. M. Smith et al., 2004; Zhang et al., 2001); the 5TT image classifies the voxel into one of 5 tissue types: cortical grey matter, sub-cortical grey matter, white matter, cerebrospinal fluid, and '5th type' (e.g. pathology). The FOD data and the 5TT image were used to generate 70 million streamlines using the anatomically constrained tractography (ACT) framework (R. E. Smith et al., 2012), using dynamic seeding (R. E. Smith et al., 2015b) and the 2nd-order Integration over Fibre Orientation Distributions (iFOD2,(Tournier et al., 2010)) probabilistic fibre-tracking algorithm, using default MRtrix parameters, with the exception of FOD cutoff 0.06, minimum streamline length 5 mm, maximum length 300 mm, and backtrack specified. This set of streamlines is referred to as the *whole-brain-tractogram* thereafter.

2.2.3. Quantitative LC-nbM pathway

The 5TT image was edited to ensure the registered nbM segmentation was classified as cortical grey matter tissue, and the LC as part of the subcortical grey matter tissue. An additional set of 25 thousand regional anatomically-constrained streamlines were generated, seeding from the LC and requiring that they should traverse the nbM (i.e., specifying the nbM as an 'include' region during tracking generation). Default tractography parameters for the regional streamlines were selected, except for seed number, which was set to zero – this ensured that 25 thousand crossing streamlines were generated between the LC and nbM (see Video 1).

The regional set of 25 thousand streamlines was concatenated with the whole-brain-tractogram, yielding a single combined set of 70,025,000 streamlines per participant of the entire brain. Spherical-deconvolution informed filtering of tractograms 2 (SIFT2, (R. E. Smith et al., 2015b)) was used on the combined set of streamlines, thereby assigning a weight to each track and providing biological credence to the quantitative connectivity measurements (Calamante, 2019; R. E. Smith et al., 2015a). Streamlines (and their associated SIFT2 weights) which traversed the LC and nbM were extracted from this combined tractogram. The resulting SIFT2 weights were summed, providing

a single connectivity measurement for the structural connectivity between the nbM and LC for each participant.

2.2.4. Average track end points between LC and nbM

Upon initial qualitative investigation of the fibre endpoints between the LC and nbM, we observed a topographical pattern of the fibre endpoints distribution in the nbM (i.e., fibres from LC to nbM) across subjects. To quantify this pattern, we employed the multivariate symmetric group-wise normalization (SyGN) method (Avants et al., 2007, 2010) to generate multimodal templates from a subset (n=13) of the HCP subjects (Lv et al., 2022). Each individual was registered to the multimodal template with the multimodal registration method (Avants et al., 2007) using their T1w, T2w, mean diffusivity and fractional anisotropy images. The warping field was recorded for each subject, and then used to register white matter tracks connecting LC and nbM into the template space. Later, the track density image (TDI) (Calamante, 2017; Calamante et al., 2010) of the track ends was generated for each registered individual and averaged across subjects to reflect the common distribution of the track ends (Dalton et al., 2021). The ROI mask of nbM was also registered into the same template space for visualization. Both the template generation and the individual warping were based on the tools implemented in the ANTs toolbox (http://stnava.github.io/ANTs/).

2.3. Functional MRI analysis

2.3.1. fMRI pre-processing

Motion correction (12 linear degrees of freedom) and bias field correction were applied to the HCP resting-state data, part of the minimally pre-processed pipeline (Glasser et al., 2013). Framewise displacement (FD) and root-mean-square change in Blood Oxygen Level-Dependent (BOLD) signal from volume to volume (DVARS) was calculated to determine the frames associated with FD > 0.05 or DVARS > 5%, and any participants with more than 20% of time points exceeding these parameters were excluded from the analysis (Power et al., 2014). The fMRI data were not 'scrubbed' due to the potential for alterations to the temporal layout of the MRI scans impacting the dynamic functional connectivity analysis (Shine et al., 2016), however we did take care to ensure that none of our outcome measures were swayed by individual differences in head motion across the cohort. Due to the presence of an evoked auditory related signal from noise in the scanner, 200 time points were discarded from the start and 100 time points removed from the end of the functional session (Shine et al., 2016). The following nuisance covariates were regressed from the time-series: twelve head movement parameters, FD, DVARS, and anatomical CompCor covariates of CSF and deep cortical white-matter (Behzadi et al., 2007). Lastly, we applied a temporal band-pass filter ($0.001 < f < 0.15$ Hz) to the data and performed normalization by z-scoring the data. One subject from the initial 50 subjects was removed from the analysis because of incomplete denoising measures, and as such we could not perform complete nuisance regression on this subject's fMRI data.

2.3.2. Region of interest selection

Following denoising, we extracted the mean time-series from 333 cortical regions of interest from the Gordon atlas (Gordon et al., 2016), as well as brainstem nuclei regions of interest from the locus coeruleus [LC] (Ye et al., 2021) and the Ch4 cholinergic cell group from the SPM Anatomy toolbox (i.e., the basal nucleus of Meynert [nbM]; ((Eickhoff et al., 2005; Zaborszky et al., 2008). As in previous work (Munn et al., 2021), we regressed signals from the nearby fourth ventricle from the LC time series prior to further analysis to ensure that these time series were not unduly effected by fluctuations in non-neural structures. We took the average time-series between the left and right ROIs of the LC, and nbM respectively.

2.3.3. Phasic increases in LC and nbM BOLD signal

Following the methodology outlined in Munn et al. (2021), we identified phasic increases in LC (T_{LC}) and nbM (T_{nbM}) BOLD signal by calculating the second derivative (i.e., acceleration) of the LC relative to the nbM increase ($T_{LC-nbM} = T_{LC} - T_{nbM}$), the nbM relative to the LC ($T_{nbM-LC} = T_{nbM} - T_{LC}$), and coherent increases of LC and nbM ($T_{LC+nbM} = T_{LC} + T_{nbM}$) time-series. In order to find points in time with strong phasic activity we used the following criteria:1) a value ≥ 2 standard deviations above the mean acceleration; 2) value of original time-series was ≥ 2 standard deviations above the mean of the time-series within the following 10TRs; and 3) the time point was not present in the first or last 20 TRs of the entire time-series. That is to say, we analysed BOLD signal in non-overlapping windows following large and sustained phasic bursts of the LC relative to nbM and nbM relative to LC.

Across all subjects, we identified 264 $T_{\text{LC - nbM}}$ phasic activity events (mean per subject was 5.38, a range of 2-10), 269 $T_{\text{nbM - LC}}$ (mean per subject was 5.49, a range of 3-10) and 271 $T_{LC+\text{ nbM}}$ (mean per subject was 5.53, range of 2-10). Our results were robust after altering the threshold between 0.5 and 2.5 standard deviations (data not shown), to further ensure the appropriate choice of standard deviation threshold was reflective of the underlying dynamics of the time-series.

2.3.4. Dynamic functional connectivity analysis

The denoised functional HCP data underwent time-series extraction for the selected ROIs. We used the multiplication of temporal derivatives (MTD) (Shine et al., 2015) to calculate time-varying functional connectivity dynamics between the selected ROIs; this method is used to estimate the functionally connectivity patterns between each region and in each time point. For each node, *n*, with time points, *t*, a vector of *t-1* temporal derivatives was calculated and normalised (temporal derivatives divided by the standard deviation of temporal derivatives, σ). Then, we created a matrix of functional coupling between the i^{th} and j^{th} nodes for each time point, by multiplying the temporal derivatives of each pair of nodes across each time point (Shine et al., 2015). A 20 TR smoothing parameter was used to then applied to the time-varying connectivity estimates so as to diminish the impact of high frequency noise (code is freely available at https://github.com/macshine/coupling/).

$$MTD_{ijt} = \frac{1}{w}\sum_{t}^{t+w}\frac{\left(dt_{it} \times dt_{jt}\right)}{\left(\sigma_{dt_i} \times \sigma_{dt_j}\right)}$$

Where dt is the first temporal derivative of the *ith* and *jth* time-series, and σ standard deviation of the temporal derivative, w is the window length of the simple moving average (Shine et al., 2015).

2.3.5. Participation coefficient

We used the Louvain algorithm to estimate a set of tightly intra-correlated modules, and then to determine the extent to which each node was integrated (functionally connected) across these different modules, we calculated the participation coefficient, B_T, for each time-resolved dynamic functional connectivity matrix (Guimerà & Nunes Amaral, 2005) using the Brain Connectivity Toolbox (BCT; (Rubinov & Sporns, 2010).

$$B_{iT} = 1 - \sum_{s=1}^{n_M}\left(\frac{K_{isT}}{K_{IT}}\right)^2$$

where $KisT$ is strength of positive connections of region i to regions in module s at specific time point T, KiT is sum of strengths of all positive connections of region i at time T. If the participation coefficient is closer to 1, connections are distributed among all modules (i.e., integration), whereas if participation coefficient is closer to 0, connections are predominantly within the regions' own module (i.e., segregation). Modules were clustered by the network assignment according to the Gordon cortical parcellation.

These data afforded a means for tracking network topology over time; however, we needed a way to link these fluctuations to changes in the activity of the arousal system hubs. To this end, we used the BOLD time series from the LC and nbM, we next estimated the cross-correlation between both LC and nbM time series and the participation coefficient

of each cortical region from the Gordon atlas (Gordon et al., 2016). The outcome of this set of analyses allowed us to track time-varying relationships between the reconfigurations in network-level whole brain topology with respect to peaks in T_{LC-nbM}, T_{nbM-LC}, and T_{LC+nbM} signal (as proxy indicators of arousal system activity), we analysed the time-to-peak of the cross-correlation between the peak signals and the 333 cortical ROIs parcels within each 10TR windows of the phasic peaks. We mapped these cross-correlation patterns onto the cortex (Fig. 3 D-F). To determine how these patterns related to the strength of white matter connections between LC and nbM, we correlated the SIFT2 weighted LC-nbM tract strength (estimated above) with the difference between the cross-correlations at each lag (0–10 TRs) (Fig. 3). The resultant correlations were tested for significance using a non-parametric permutation test that scrambled the order of the subjects' data (5,000 permutations; $p < 0.05$; (Nichols & Holmes, 2002)).

2.3.6. Brain-state displacement and attractor landscape

In order to evaluate the changes of BOLD activity in relation to phasic bursts in neuromodulatory activity, we utilised the approach introduced in Munn et al., 2021 (code for this analysis available https://github.com/ShineLabUSYD/Brainstem_DTI_Attractor_Paper). Briefly, this approach estimates the likelihood that a given brain state will changes into another distinct brain state, within a given time window. Specifically, this involves calculating the mean-squared displacement (MSD; the mean squared difference between 2 periods in time) for each combination of brain states (i.e., the configuration of BOLD patterns across all regions at a given TR) – the higher the difference between the two states, the higher the MSD value. We separately estimate the empirical probability of the change, in which higher changes are less likely to occur within shorter time windows. From these data, we estimate a probability distribution, and then invert this value to estimate the energy needed to overcome an energy barrier to facilitate the brain state change (or what energy the brain needs to move from one state to the other).

We inferred the topography of the attractor landscape by examining the likelihood of changes in the instantaneous BOLD signal (brain-state) following phasic bursts of the LC and nbM. Changes in BOLD signal were quantified using the BOLD mean-squared displacement (MSD) across varying time-lags t. First, we calculated the mean squared displacement (MSD), which measures the deviation of the BOLD activity for r nodes, in relation to activity of the phasic onset, t_0. For different t_0, where t_0 are the onset of neuromodulatory phasic bursts, across t TRs, we calculate the average change of each voxel, $<>_r$ is the mean across the nodes.

$$MSD_{t,t_0} = \left\langle \left| x_{t_0+t} - x_{t_0} \right|^2 \right\rangle_r.$$

Then, we estimated the probability of a BOLD displacement at a time-lag t, $P(MSD_t)$. The probability distribution was calculated from n MSD_{t,t_0} samplings (n being the number of phasic onset, t_0 of the neuromodulatory systems) by a Gaussian kernel density estimation,

$$P\left(MSD_t\right) = \frac{1}{4n}\sum_{i=1}^{n} K\left(\frac{MSD_{t,t_0(i)}}{4}\right)$$

and we calculated the probability distribution for t between 1 and 19TR and MSD between 0 and 11. We then calculated the energy, E, of BOLD MSD attractor state at a given time-lag t, as the natural logarithm of the inverse probability:

$$E = \ln\left(\frac{1}{P\left(MSD_t\right)}\right)$$

This approach indicates that a highly probable relative change in BOLD (calculated by MSD) corresponds to a low energy (i.e., small E), and an unlikely change in BOLD requires a higher energy (i.e., large E) (Munn et al., 2021).

We calculated the BOLD MSD following phasic bursts of T_{LC-nbM} (LC relative to nbM) - E_{LC}, T_{nbM-LC} (nbM relative to LC) - E_{nbM}, T_{LC+nbM} (simultaneous phasic peaks of LC and nbM) – E_{LC+nbM}, and BOLD MSD outside of the phasic bursts of the three signals (i.e., outside ± 20 TR from phasic bursts), defined as the baseline energy landscape E_A. The energy landscapes calculated following phasic bursts of T_{LC-nbM}, T_{nbM-LC}, or T_{LC+nbM} are presented relative to the inferred baseline MSD energetics (E_A), i.e., E_X - E_A. Subtracting the baseline is similar to a residual in Energy MSD/TR space and is calculated to emphasise the differences in the BOLD transitions following the phasic bursts. The attractor landscapes are represented as the energy for a given MSD at a given temporal displacement (TR) (Fig. 4).

2.3.7. Relationship between attractor landscape and LC and nbM structural connectivity

In order to determine the relationship between the attractor landscape brain states and the underlying structural connectivity between the LC and nbM, we calculated the Pearson correlation between the weighted strength in structural connectivity between the LC and nbM, and the energy associated with a given MSD/TR combination following phasic activity within the LC (E_{LC}), nbM (E_{nbM}), LC and nbM combined (E_{LC+nbM}) for each subject. To further extend this analysis, we calculated the gradient of the energy post-phasic LC and nbM activity, to determine the extent of the change in the energy for a given MSD of BOLD signal across the TRs. We calculated the gradient as the partial derivative of the energy for a given MSD of the BOLD signal across TRs (using MATLAB Version 2021a, function gradient).

2.3.8. Statistical analyses

For statistical analysis, we performed non-parametric permutation testing to compare our data across 5,000 random iterations. Permutation testing computes all possible values of the test statistic under random reorganizations of the observed data, through randomization of the labels For example, we randomly changed the 'phasic burst' timing of each neuromodulatory system, to measure if the empirical correlation was higher (or lower) in comparison to the null permutated distribution. Statistical significance represents the 2.5^{th} and 97.5^{th} percentile of the null distribution from the non-parametric permutation test (Nichols & Holmes, 2002).

3. Results

3.1. Quantitative structural connectivity between the LC and nbM

We observed a topographic pattern of crossing fibre ends tracking from the LC to terminate in the nbM. Specifically, we observed a greater distribution of fibre ends (group averaged) along the medial border of the axial plane of the nbM mask. We also observed bilateral differences in the density of fibre ends, with a greater density terminating in the right nbM (Video 2). In addition, a similar medial dominant distribution of fibre ends in the nbM was also observed in the coronal plane (Fig. 2C). The distribution of the fibre ends in the nbM changed across slices, as we observed a more 'clumped' density of fibres ends moving dorsally (Video 2, Fig. 2C).

3.2. Neuromodulatory burst in activity precedes network topological shifts relating to structural connectivity between LC and nbM

In order to track time-varying relationships between bursts in neuromodulatory activity and reconfigurations in network-level topology, we analysed the cross-correlation between neuromodulatory phasic bursts and the cortical regions within 10 TR of the phasic peaks. Then, we determined how these patterns related to the underlying white matter connections between the LC and nbM by calculating the correlation between structural strength in connectivity with the difference between the cross-correlations at each time lag. In this way, we were able to determine whether the underlying strength in white matter streamlines between LC and nbM relate to the time-varying reconfigurations

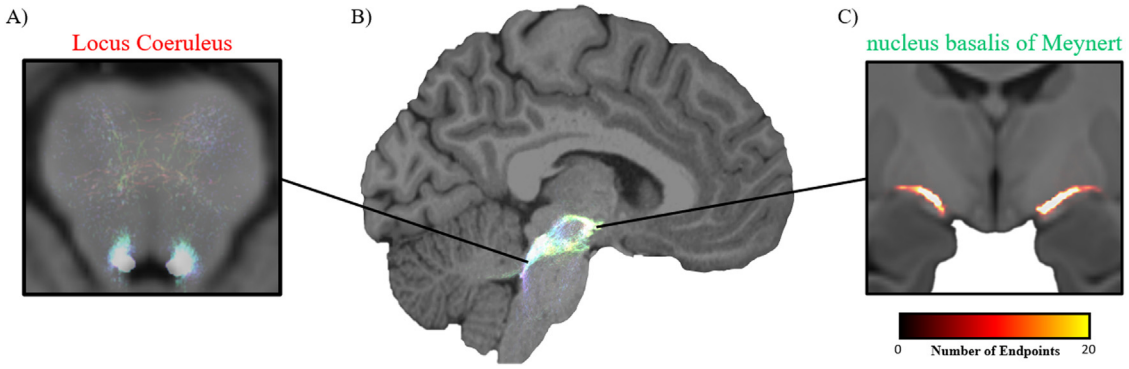

Fig. 2. Diffusion tractography streamlines between the LC and nbM. A single subject's white matter crossing streamline consolidated around the LC (A). Representation of a single subject's white matter streamlines between LC (red) to nbM (green) from diffusion imaging (B) (3D view of streamlines in video 1). The fibre orientation of the streamlines in accordance with the colour is red: left – right, green: dorsal – ventral, blue: cranial – caudal. Video 1 shows the view of the white matter streamlines from LC to nbM for a single subject. A coronial view of the average fibre ends in the nbM (fibres tracking from LC to nbM), density indicated by the contrast in colour intensity from black ranging to yellow (C). Video 2 shows the axial plane of the average fibre ends in the nbM (fibres tracking from LC to nbM), moving from inferior slices to superior slices.

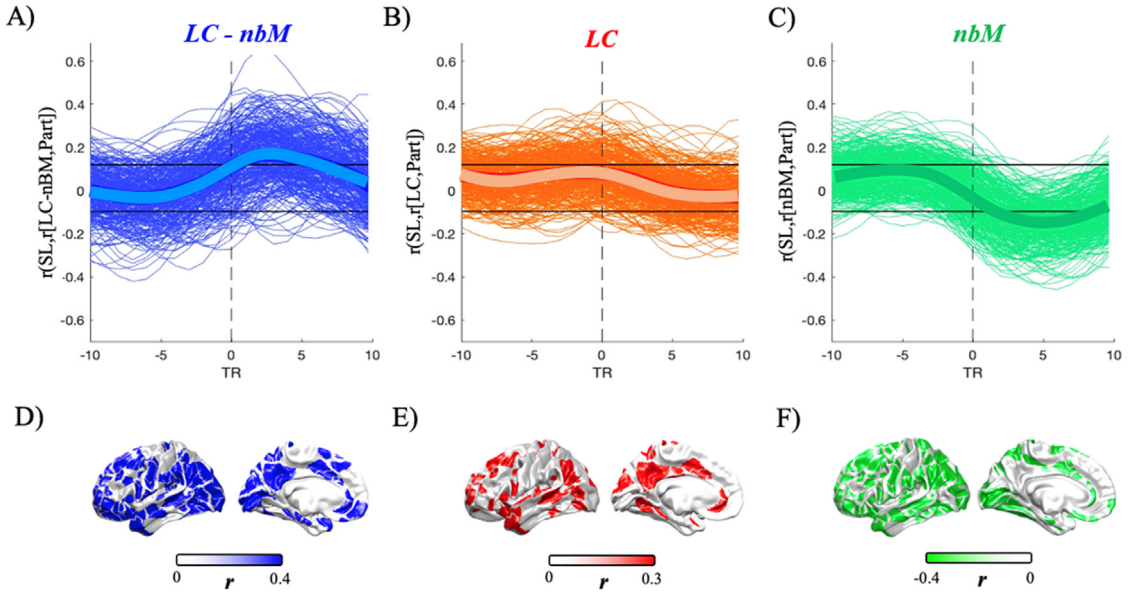

Fig. 3. Relationship between weighted streamlines and arousal-related network reconfiguration. Correlation (y-axis) between weighted streamlines from LC to nbM (SL) with the difference between cross-correlations at each time lag. The cross-correlation was between LC-nbM (A: blue) (r[LC-nbM,part]), LC (B; red) (r[LC,part]), and nbM (C; green) (r[nbM,part]) phasic activity and cortical regional participation coefficient. Thin lines represent individual regions and thick lines represent the grand mean across all regions. The dotted lines designate the zero-lagged correlation, and the thick black lines designate the 2.5th and 97.5th percentile of the null distribution from the non-parametric permutation test (5,000 iterations). D-F) surface plots of the peak in time-lagged correlation between each of the three subcortical signals and regional participation.

of network-level topology following bursts in neuromodulatory activity. The weight of white matter connections between the LC and nbM was positively correlated with the extent of network-level integration following LC relation to nbM phasic bursts (Fig. 3; left). These results suggest that strong connectivity between the LC and nbM allows the network to shift towards a heightened level of integration following peaks in LC relative to nbM activity. We observed increased integration following peaks in LC relative to nbM activity across several regions in the cortex including fronto-parietal and visual cortex (Fig. 3D). To further investigate this result, we interrogated the correlation between the total weighted streamlines connectivity and the individual cross-correlations between LC (Fig. 3; middle) or nbM phasic bursts (Fig. 3; right) and network topology. Interestingly, we observed significant negative correlations between post-nbM peaks and a strongly segregated network state (Fig. 3C) across distributed regions in the cortex (Fig. 3F).

3.3. Neuromodulation of attractor landscapes

To further investigate the dynamic role of the noradrenergic and cholinergic system, we investigated the role of phasic activity of the neuromodulators in modifying the attractor landscape of the brain. Based on previous work (Munn et al., 2021), we hypothesised that the noradrenergic system would 'flatten' the attractor landscape (promoting higher energy brain-state changes by increasing the likelihood for these rare states to occur) whereas the cholinergic system would 'deepen the wells' of the attractor landscape (decreasing the likelihood of large brain-state changes). To test our hypothesis, we calculated the MSD energetics following phasic bursts of LC relative to nbM (E_{LC}), nbM relative to LC (E_{nbM}), and simultaneous phasic burst of LC and nbM (E_{LC+nbM}), all relative to the baseline MSD energetics (E_A) outside of these regimes. The phasic bursts were defined as peaks in the second derivative of the

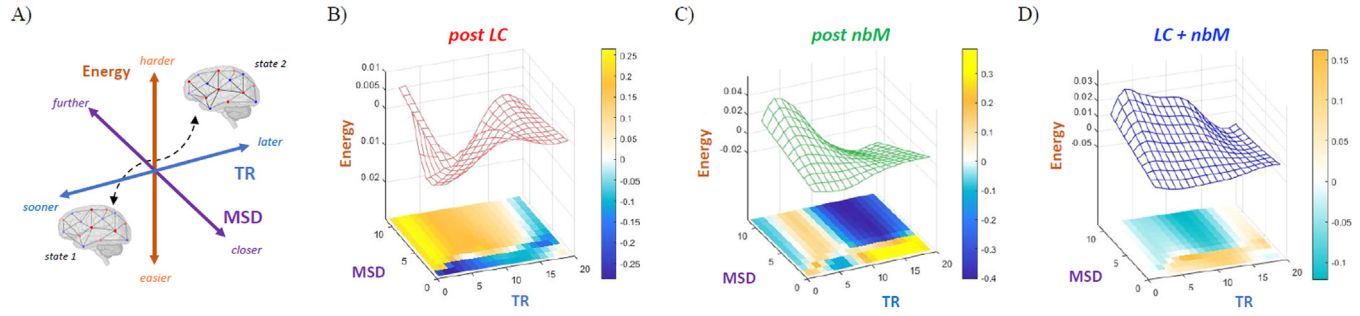

Fig. 4. Relationship between attractor landscape of the brain and underlying structural connectivity between the noradrenergic and cholinergic systems. A) Visual representation of the three-dimensional attractor landscape plot; the y-axis describes the likelihood (energy) required to shift brain states, x-axis describes the time-lag following phasic bursts, and the z-axis describes the brain-state transition (mean-squared displacement). (Top) The attractor landscapes demonstrate the likelihood to observe a given brain-state transition (quantified by the mean-squared displacement [MSD]) at a given time-lag (TR) following phasic bursts of the LC relative to nbM (B; red), nbM relative to LC (C; green), or both simultaneously LC + nbM (D; blue). (Bottom) The bottom 2D plots display the correlation (Pearson's correlation Rho values represented by colour bar) between the weighted strength in structural connectivity between the LC and nbM, and the energy for a given MSD of BOLD signal post phasic activity of the LC (E_{LC}-E_A) (B; red), nbM (E_{nbM}-E_A) (C; green), and LC + nbM combined (E_{LC+nbM}-E_A) (D; blue) relative to baseline. The opacity represents the statistical significance; opaque colours represent correlations that fell within the 2.5th and 97.5th percentile of the null distribution from the non-parametric permutation test (5,000 iterations) – i.e., opaque regions (bold colours) of the matrix were considered significant at the $p < 0.05$ level.

respective neuromodulatory BOLD signal that resulted in a sustained increased BOLD activity across each subject (see Methods).

To determine the relationship between the structural connectivity between the LC and nbM and shifts in the attractor landscape, we calculated the permutated (5,000 random iterations) correlation between each subject's attractor landscapes following phasic burst in the LC and nbM across time, and the weighted connectivity between the LC and nbM. We observed a significant positive correlation between the post LC phasic activity, the energy landscape (E_{LC}) and the strength in connectivity between the LC and nbM that was localised within a 2 TR window after the phasic burst (Fig. 4B). This finding suggests that immediately after LC phasic bursts, an individual with strong connections between LC and nbM is unlikely to have large deviations in brain state dynamics. In contrast, we observed a significant inverse correlation post nbM phasic activity (post 11TR, >8s), between the strength in connectivity between the LC and nbM, and the energy landscape (E_{nbM}) (Fig. 4C), which indicates that post nbM phasic bursts, having strong connections between the LC and nbM enables an easier shift (i.e., there is lower energy required to shift into a previously rare brain state). The largest correlations are seen between E_{LC} at the onset of the initial dip for large MSD at early TR and for the dip of large MSD at large TR for the E_{nbM} landscape. Thus, the strength in structural connectivity between the LC and nbM is associated with the greatest change in energy for a given MSD of BOLD signal post LC or nbM phasic activity – i.e., the topography of the attractor landscape correlates with the strength of the structural connectivity.

4. Discussion

We showed that the strength of structural connectivity between the cholinergic nbM and noradrenergic LC was related to fluctuations in network topology and attractor topography estimated from resting state fMRI data. Our findings support a previous experimental finding that the cholinergic and noradrenergic system is related to the ability to shift network topological states (Munn et al., 2021; Shine, 2019). Furthermore, we established a topographic distribution of crossing fibre ends from the LC to the nbM, which was consistent with previous histological studies showing more pronounced and direct noradrenergic projections to the nbM (Hajszán & Zaborszky, 2002; Smiley et al., 1999; Zaborszky et al., 1993). Future work will interrogate the unilateral topographic distribution of fibres ends from the LC to nbM. Whilst previously it has been challenging to delineate the structural connectivity of these small brainstem nuclei, recent advancements in tractography algorithms have enabled several studies to reliably track LC white-matter structural connectivity (Solders et al., 2022; Sun et al., 2020). These results provide evidence for the importance of the ascending arousal system in shaping and constraining emergent dynamics in the brain.

There is compelling evidence to suggest that the balance between integration and segregation is already partially imbued by the structure of the white matter connectivity backbone of the cerebral cortex (Park & Friston, 2013; Sporns, 2013). Specifically, local cellular connections support segregation, whereas broad-reaching axonal projections spanning different cortical regions act to integrate neural signals by constraining the coordinated interactions between functional networks (Bullmore & Sporns, 2009, 2012). Our results demonstrate that these inherent features of the structural connectome are adaptively augmented by dynamic constraints imbued by the ascending arousal system. Specifically, we extended upon previous work (Munn et al., 2021) by showing that the network shifts into an integrated state following LC relative to nbM phasic activity (Fig. 3; left). Furthermore, these patterns were observed to covary with the strength of structural connectivity between the LC and nbM, in which we observed a significant negative correlation between the post-nbM peaks (Fig. 3; right), suggesting that heightened structural connectivity between the LC and nbM allows the brain to integrate, but also stabilise into a relatively segregated state following a relatively large recruitment of the nbM (which may be controlled by other factors, such as the activity of the surrounding network (Alves et al., 2019) and resting cholinergic tone (Hasselmo, 2006; Teles-Grilo Ruivo et al., 2017).

More broadly, our findings extend a body of work that seeks to clarify the underlying neural mechanisms responsible for the modulation of macro-scale neural dynamics of the brain (Kanamaru & Aihara, 2019; Munn et al., 2021; Shine et al., 2021b; Shine & Poldrack, 2018; Watanabe, 2021; Watanabe et al., 2014). Specifically, we have provided further evidence that the brain's neural dynamics can be explained through low-dimensional, dynamically-shifting energy landscapes (Munn et al., 2021). Our findings extend results from a previous study (Munn et al., 2021), as underlying structural connectivity between the cholinergic and noradrenergic system relates to the ability to have a balance between the flattened and deepened-well energy landscape of the brain. Our findings propose that the underlying strength in connectivity between the neuromodulatory hubs gives rise to modulation of dynamic network topology, in which initially post LC phasic activity there is lower probability of large deviations ('deepened-wells') in the attractor landscape of the brain relative to the interconnectivity between the LC and nbM. On the contrary, the strength in structural connectivity between the LC and nbM was inversely related to the post nbM phasic activity, indicating that a stronger connection between the neuromodu-

latory hubs facilitates a lower energy requirement (i.e., greater probability) of the attractor landscape to shift into difficult brain states post nbM activity. As such, our study further evidences the contributions of the underlying structural connectome in modulating the dynamic functional connectivity.

This study joins a growing body of work that evidences the interaction between noradrenergic and cholinergic neuromodulation mediates the balance between segregated and integrated brain states (Shine, 2019). The dynamic flexibility between the integrated and segregated states has important implications for cognitive function. Previous research has established that the ability to shift into an integrated state is mediated through noradrenergic administration, and confers with cognitive performance (Shine, van den Brink, et al., 2018). More specifically, the LC-mediated flattening of the energy landscape is similar to the theory of alpha-1 receptor-mediated network reset (Sara & Bouret, 2012), and builds upon previous work theorising that the noradrenergic system through second-messenger cascades (Shine et al., 2021b) increases the response gain and coordinates integrated network connectivity (Shine, Aburn, et al., 2018). This interaction has relevant implications to cognitive neuroscience in which the capacity to flexibly adapt to unexpected changes in the environment in the context of flattening the landscape could facilitate flexible cognitive processes (Aston-Jones & Cohen, 2005; Munn et al., 2021; Sara & Bouret, 2012), whereas the cholinergic system mediates segregated network topology through its localised selective projections to the cortex (Zaborszky et al., 2015) through the selective augmentation of the excitability of target regions within otherwise distributed networks (Shine, 2019; Thiele & Bellgrove, 2018). This mechanism is argued to help refine the stability of brain states, which in the context of cognitive function, could help to explain why the cholinergic system is associated with heightened attentional precision (Hasselmo & Sarter, 2011; Schmitz & Duncan, 2018). Unravelling the complexity of the interactions between the noradrenergic and cholinergic system on attractor landscapes, particularly in the context of cognitive task performance has the potential to augment our broader understanding of how the distributed neural circuits of the brain support cognitive function. However, there are inherent limitations with our work as we have a limited number of subjects with a relatively new analysis technique. Future work will expand the new analysis methods to larger sample populations to further validate our approach.

The complexity of the interactions between the noradrenergic and cholinergic system in modulating network topological shifts is still not fully understood at a detailed (i.e., microcircuit) level. For instance, there is ample evidence for heterogeneous expression of cholinergic receptors across different inhibitory interneuron populations (Que et al., 2019), suggesting that there may be more subtle mechanisms at play in the microcircuitry of the cerebral cortex, however many of these details are not incorporated into standard computational models of systems-level brain dynamics (John et al., 2022; Shine et al., 2019). The flexibility of this approach offers a number of exciting opportunities for progress on this front. For instance, a recent study included an 'inhibitory gain' term to an existing computational model to mimic the effects of the cholinergic system – this allowed the control of both inhibitory and disinhibitory interneurons, which in turn controlled feedback excitation in a manner that provided tighter control over the balance between segregation and integration (Coronel-Oliveros et al., 2020). It is also highly likely that neuromodulatory transmitters other than the cholinergic and noradrenergic systems are responsible for nuanced alterations in dynamic network reconfigurations. For instance, numerous studies have demonstrated that agonists of 5HT2A receptor (typically classed as 'psychedelics') cause substantial alterations in brain network dynamics (Herzog et al., 2020; Tagliazucchi et al., 2016) and energy landscape topography (Singleton et al., 2021). Future studies are required to compare and contrast these different signatures across the pharmacological landscape. Finally, other complex features of neuroanatomy could contribute to dynamic shifts in brain states – for example, different classes of thalamocortical projections could be critical in promoting dynamic evolving attractor landscapes and mediates multiscale network organization (Shine, 2021). We look forward to further research that we believe will help to unravel the details governing modulation of neural dynamics at the macroscale.

5. Conclusion

In conclusion, we replicate and extend previous work that show a strong link between the ascending arousal system and network-level dynamic reconfiguration in the human brain. Our results highlight the importance of underlying structural connectivity between the cholinergic and noradrenergic system in facilitating reconfiguration of network topology, which could have important implications in understanding the role of the ascending arousal system in facilitating adaptive neural reconfiguration as a function of cognitive demands.

Data & code availability

All data is available through the open-access Human Connectome Project, from the WU-Minn HCP (Van Essen et al., 2013) 100 unrelated subject cohort. Code for the analysis is available https://github.com/ShineLabUSYD/Brainstem_DTI_Attractor_Paper.

Credit author statement

NLT, BM, AD, GW, LZ, FC and JMS conceptualized the study.
NLT, AD, JL and BM preprocessed and analysed the imaging data.
NLT and JMS wrote the initial draft.
All co-authors edited the final manuscript.

Declarations of Competing Interest

None.

Acknowledgements

We acknowledge the data made available through the Human Connectome Project, WU-Minn Consortium (Principal Investigators: David Van Essen and Kamil Ugurbil; 1U54MH091657) funded by the 16 NIH Institutes and Centers that support the NIH Blueprint for Neuroscience Research; and by the McDonnell Center for Systems Neuroscience at Washington University.

We acknowledge the technical assistance provided by the Sydney Informatics Hub and Sydney Imaging, two Core Research Facilities of The University of Sydney.

JMS is supported by an NHMRC Project Grant (#1193857) and University of Sydney Robinson Fellowship. FC is supported by the NHMRC (#APP1117724) and ARC (#DP170101815).

Supplementary materials

Supplementary material associated with this article can be found, in the online version, at doi:10.1016/j.neuroimage.2022.119455.

References

Alcedo, J., Prahlad, V., 2020. Neuromodulators: an essential part of survival. J. Neurogenet. 34 (3–4), 475–481. doi:10.1080/01677063.2020.1839066.

Alves, P.N., Foulon, C., Karolis, V., Bzdok, D., Margulies, D.S., Volle, E., de Schotten, M.T., 2019. Subcortical anatomy of the default mode network: a functional and structural connectivity study. [Preprint]. Neuroscience doi:10.1101/528679.

Andersson, J.L.R., Skare, S., Ashburner, J., 2003. How to correct susceptibility distortions in spin-echo echo-planar images: Application to diffusion tensor imaging. Neuroimage 20 (2), 870–888. doi:10.1016/S1053-8119(03)00336-7.

Andersson, J.L.R., Sotiropoulos, S.N., 2015. Non-parametric representation and prediction of single- and multi-shell diffusion-weighted MRI data using Gaussian processes. Neuroimage 122, 166–176. doi:10.1016/j.neuroimage.2015.07.067.

Andersson, J.L.R., Sotiropoulos, S.N., 2016. An integrated approach to correction for off-resonance effects and subject movement in diffusion MR imaging. Neuroimage 125, 1063–1078. doi:10.1016/j.neuroimage.2015.10.019.

Aston-Jones, G., Cohen, J.D., 2005. An integrative theory of locus coeruleus-norepinephrine function: adaptive gain and optimal performance. Annu. Rev. Neurosci. 28 (1), 403–450. doi:10.1146/annurev.neuro.28.061604.135709.

Avants, B.B., Duda, J.T., Zhang, H., Gee, J.C., 2007. Multivariate normalization with symmetric diffeomorphisms for multivariate studies. In: Medical Image Computing and Computer-Assisted Intervention: MICCAI ... International Conference on Medical Image Computing and Computer-Assisted Intervention, 10, pp. 359–366. doi:10.1007/978-3-540-75757-3_44.

Avants, B.B., Tustison, N.J., Song, G., Cook, P.A., Klein, A., Gee, J.C., 2011. A reproducible evaluation of ANTs similarity metric performance in brain image registration. Neuroimage 54 (3), 2033–2044. doi:10.1016/j.neuroimage.2010.09.025.

Avants, B.B., Yushkevich, P., Pluta, J., Minkoff, D., Korczykowski, M., Detre, J., Gee, J.C., 2010. The optimal template effect in hippocampus studies of diseased populations. Neuroimage 49 (3), 2457–2466. doi:10.1016/j.neuroimage.2009.09.062.

Bassett, D.S., Wymbs, N.F., Porter, M.A., Mucha, P.J., Carlson, J.M., Grafton, S.T., 2011. Dynamic reconfiguration of human brain networks during learning. Proc. Natl. Acad. Sci. 108 (18), 7641–7646. doi:10.1073/pnas.1018985108.

Bassett, D.S., Yang, M., Wymbs, N.F., Grafton, S.T., 2015. Learning-induced autonomy of sensorimotor systems. Nat. Neurosci. 18 (5), 744–751. doi:10.1038/nn.3993.

Behzadi, Y., Restom, K., Liau, J., Liu, T.T., 2007. A component based noise correction method (CompCor) for BOLD and perfusion based fMRI. Neuroimage 37 (1), 90–101. doi:10.1016/j.neuroimage.2007.04.042.

Braun, U., Schäfer, A., Walter, H., Erk, S., Romanczuk-Seiferth, N., Haddad, L., Schweiger, J.I., Grimm, O., Heinz, A., Tost, H., Meyer-Lindenberg, A., Bassett, D.S., 2015. Dynamic reconfiguration of frontal brain networks during executive cognition in humans. Proc. Natl. Acad. Sci. 112 (37), 11678–11683. doi:10.1073/pnas.1422487112.

Brown, E.N., Purdon, P.L., Van Dort, C.J., 2011. General anesthesia and altered states of arousal: a systems neuroscience analysis. Annu. Rev. Neurosci. 34 (1), 601–628. doi:10.1146/annurev-neuro-060909-153200.

Bullmore, E., Sporns, O., 2009. Complex brain networks: Graph theoretical analysis of structural and functional systems. Nat. Rev. Neurosci. 10 (3), 186–198. doi:10.1038/nrn2575.

Bullmore, E., Sporns, O., 2012. The economy of brain network organization. Nat. Rev. Neurosci. 13 (5), 336–349. doi:10.1038/nrn3214.

Calamante, F., 2017. Track-weighted imaging methods: Extracting information from a streamlines tractogram. MAGMA 30 (4), 317–335. doi:10.1007/s10334-017-0608-1.

Calamante, F., 2019. The seven deadly sins of measuring brain structural connectivity using diffusion MRI streamlines fibre-tracking. Diagnostics 9 (3), E115. doi:10.3390/diagnostics9030115.

Calamante, F., Tournier, J.-D., Jackson, G.D., Connelly, A., 2010. Track-density imaging (TDI): super-resolution white matter imaging using whole-brain track-density mapping. Neuroimage 53 (4), 1233–1243. doi:10.1016/j.neuroimage.2010.07.024.

Carter, M.E., Yizhar, O., Chikahisa, S., Nguyen, H., Adamantidis, A., Nishino, S., Deisseroth, K., de Lecea, L., 2010. Tuning arousal with optogenetic modulation of locus coeruleus neurons. Nat. Neurosci. 13 (12), 1526–1533. doi:10.1038/nn.2682.

Castro-Alamancos, M.A., Gulati, T., 2014. Neuromodulators produce distinct activated states in neocortex. J. Neurosci. 34 (37), 12353–12367. doi:10.1523/JNEUROSCI.1858-14.2014.

Catani, M., Thiebautdeschotten, M., 2008. A diffusion tensor imaging tractography atlas for virtual in vivo dissections. Cortex 44 (8), 1105–1132. doi:10.1016/j.cortex.2008.05.004.

Civier, O., Smith, R.E., Yeh, C.-H., Connelly, A., Calamante, F., 2019. Is removal of weak connections necessary for graph-theoretical analysis of dense weighted structural connectomes from diffusion MRI? Neuroimage 194, 68–81. doi:10.1016/j.neuroimage.2019.02.039.

Cohen, J.R., D'Esposito, M, 2016. The segregation and integration of distinct brain networks and their relationship to cognition. J. Neurosci. 36 (48), 12083–12094. doi:10.1523/JNEUROSCI.2965-15.2016.

Coronel-Oliveros, C., Cofré, R., Orio, P., 2020. Cholinergic neuromodulation of inhibitory interneurons facilitates functional integration in whole-brain models. [Preprint]. Neuroscience doi:10.1101/2020.09.04.282095.

Dalton, M.A., D'Souza, A., Lv, J., Calamante, F, 2021. Anatomical connectivity along the anterior-posterior axis of the human hippocampus: new insights using quantitative fibre-tracking. p. 2021.11.17.469032. bioRxiv doi:10.1101/2021.11.17.469032.

Eickhoff, S.B., Stephan, K.E., Mohlberg, H., Grefkes, C., Fink, G.R., Amunts, K., Zilles, K., 2005. A new SPM toolbox for combining probabilistic cytoarchitectonic maps and functional imaging data. Neuroimage 25 (4), 1325–1335. doi:10.1016/j.neuroimage.2004.12.034.

Fransson, P., Schiffler, B.C., Thompson, W.H., 2018. Brain network segregation and integration during an epoch-related working memory fMRI experiment. Neuroimage 178, 147–161. doi:10.1016/j.neuroimage.2018.05.040.

Glasser, M.F., Sotiropoulos, S.N., Wilson, J.A., Coalson, T.S., Fischl, B., Andersson, J.L., Xu, J., Jbabdi, S., Webster, M., Polimeni, J.R., Van Essen, D.C., Jenkinson, M., 2013. The minimal preprocessing pipelines for the Human Connectome Project. Neuroimage 80, 105–124. doi:10.1016/j.neuroimage.2013.04.127.

Gordon, E.M., Laumann, T.O., Adeyemo, B., Huckins, J.F., Kelley, W.M., Petersen, S.E., 2016. Generation and evaluation of a cortical area parcellation from resting-state correlations. Cereb. Cortex 26 (1), 288–303. doi:10.1093/cercor/bhu239.

Guimerà, R., Nunes Amaral, L.A., 2005. Functional cartography of complex metabolic networks. Nature 433 (7028), 895–900. doi:10.1038/nature03288.

Hajszán, T., Zaborszky, L., 2002. Direct catecholaminergic–cholinergic interactions in the basal forebrain. III. Adrenergic innervation of choline acetyltransferase-containing neurons in the rat. J. Comp. Neurol. 449 (2), 141–157. doi:10.1002/cne.10279.

Hasselmo, M.E., 2006. The role of acetylcholine in learning and memory. Curr. Opin. Neurobiol. 16 (6), 710–715. doi:10.1016/j.conb.2006.09.002.

Hasselmo, M.E., Sarter, M., 2011. Modes and models of forebrain cholinergic neuromodulation of cognition. Neuropsychopharmacology 36 (1), 52–73. doi:10.1038/npp.2010.104.

Hearne, L.J., Cocchi, L., Zalesky, A., Mattingley, J.B., 2017. Reconfiguration of brain network architectures between resting-state and complexity-dependent cognitive reasoning. J. Neurosci. 37 (35), 8399–8411. doi:10.1523/JNEUROSCI.0485-17.2017.

Herzog, R., Mediano, P.A.M., Rosas, F.E., Carhart-Harris, R., Perl, Y.S., Tagliazucchi, E., Cofre, R., 2020. A mechanistic model of the neural entropy increase elicited by psychedelic drugs. Sci. Rep. 10 (1), 17725. doi:10.1038/s41598-020-74060-6.

Honey, C.J., Sporns, O., Cammoun, L., Gigandet, X., Thiran, J.P., Meuli, R., Hagmann, P., 2009. Predicting human resting-state functional connectivity from structural connectivity. Proc. Natl. Acad. Sci. 106 (6), 2035–2040. doi:10.1073/pnas.0811168106.

Ito, T., Hearne, L.J., Cole, M.W., 2020. A cortical hierarchy of localized and distributed processes revealed via dissociation of task activations, connectivity changes, and intrinsic timescales. Neuroimage 221, 117141. doi:10.1016/j.neuroimage.2020.117141.

Jeurissen, B., Tournier, J.-D., Dhollander, T., Connelly, A., Sijbers, J., 2014. Multi-tissue constrained spherical deconvolution for improved analysis of multi-shell diffusion MRI data. Neuroimage 103, 411–426. doi:10.1016/j.neuroimage.2014.07.061.

John, Y.J., Sawyer, K.S., Srinivasan, K., Müller, E.J., Munn, B.R., Shine, J.M., 2022. It's about time: Linking dynamical systems with human neuroimaging to understand the brain. Netw. Neurosci. 1–54. doi:10.1162/netn_a_00230.

Kanamaru, T., Aihara, K., 2019. Acetylcholine-mediated top-down attention improves the response to bottom-up inputs by deformation of the attractor landscape. PLoS One 14 (10), e0223592. doi:10.1371/journal.pone.0223592.

Kim, J.-H., Jung, A.-H., Jeong, D., Choi, I., Kim, K., Shin, S., Kim, S.J., Lee, S.-H., 2016. Selectivity of neuromodulatory projections from the basal forebrain and locus ceruleus to primary sensory cortices. J. Neurosci. 36 (19), 5314–5327. doi:10.1523/JNEUROSCI.4333-15.2016.

Lee, S.-H., Dan, Y., 2012. Neuromodulation of brain states. Neuron 76 (1), 209–222. doi:10.1016/j.neuron.2012.09.012.

Lin, S.-C., Brown, R.E., Hussain Shuler, M.G., Petersen, C.C.H., Kepecs, A., 2015. Optogenetic dissection of the Basal Forebrain Neuromodulatory control of cortical activation, plasticity, and cognition. J. Neurosci. 35 (41), 13896–13903. doi:10.1523/JNEUROSCI.2590-15.2015.

Lv, J., Zeng, R., Ho, M.P., D'Souza, A., Calamante, F, 2022. Building a tissue-unbiased brain template of fibre orientation distribution and tractography with multimodal registration. p. 2022.04.13.488117. bioRxiv doi:10.1101/2022.04.13.488117.

Marder, E., 2012. Neuromodulation of neuronal circuits: back to the future. Neuron 76 (1), 1–11. doi:10.1016/j.neuron.2012.09.010.

McGinley, M.J., Vinck, M., Reimer, J., Batista-Brito, R., Zagha, E., Cadwell, C.R., Tolias, A.S., Cardin, J.A., McCormick, D.A., 2015. Waking state: rapid variations modulate neural and behavioral responses. Neuron 87 (6), 1143–1161. doi:10.1016/j.neuron.2015.09.012.

Mei, J., Muller, E., Ramaswamy, S., 2022. Informing deep neural networks by multiscale principles of neuromodulatory systems. Trend. Neurosci. 45 (3), 237–250. doi:10.1016/j.tins.2021.12.008.

Mena-Segovia, J., Sims, H.M., Magill, P.J., Bolam, J.P., 2008. Cholinergic brainstem neurons modulate cortical gamma activity during slow oscillations: cholinergic neurons during slow wave activity. J. Physiol. 586 (12), 2947–2960. doi:10.1113/jphysiol.2008.153874.

Mišić, B., Betzel, R.F., de Reus, M.A., van den Heuvel, M.P., Berman, M.G., McIntosh, A.R., Sporns, O., 2016. Network-level structure-function relationships in human neocortex. Cereb. Cortex (New York, NY) 26 (7), 3285–3296. doi:10.1093/cercor/bhw089.

Mohr, H., Wolfensteller, U., Betzel, R.F., Mišić, B., Sporns, O., Richiardi, J., Ruge, H., 2016. Integration and segregation of large-scale brain networks during short-term task automatization. Nat. Commun. 7 (1), 13217. doi:10.1038/ncomms13217.

Müller, E.J., Munn, B.R., Shine, J.M., 2020. Diffuse neural coupling mediates complex network dynamics through the formation of quasi-critical brain states. Nat. Commun. 11 (1), 6337. doi:10.1038/s41467-020-19716-7.

Munn, B.R., Müller, E.J., Wainstein, G., Shine, J.M., 2021. The ascending arousal system shapes neural dynamics to mediate awareness of cognitive states. Nat. Commun. 12 (1), 6016. doi:10.1038/s41467-021-26268-x.

Nichols, T.E., Holmes, A.P., 2002. Nonparametric permutation tests for functional neuroimaging: a primer with examples. Hum. Brain Mapp. 15 (1), 1–25. doi:10.1002/hbm.1058.

Noudoost, B., Moore, T., 2011. The role of neuromodulators in selective attention. Trends Cogn. Sci. 15 (12), 585–591. doi:10.1016/j.tics.2011.10.006.

Park, H.-J., Friston, K., 2013. Structural and functional brain networks: from connections to cognition. Science 342 (6158), 1238411. doi:10.1126/science.1238411.

Patenaude, B., Smith, S.M., Kennedy, D.N., Jenkinson, M., 2011. A Bayesian model of shape and appearance for subcortical brain segmentation. Neuroimage 56 (3), 907–922. doi:10.1016/j.neuroimage.2011.02.046.

Patil, A.U., Ghate, S., Madathil, D., Tzeng, O.J.L., Huang, H.-W., Huang, C.-M., 2021. Static and dynamic functional connectivity supports the configuration of brain networks associated with creative cognition. Sci. Rep. 11 (1), 165. doi:10.1038/s41598-020-80293-2.

Power, J.D., Mitra, A., Laumann, T.O., Snyder, A.Z., Schlaggar, B.L., Petersen, S.E., 2014. Methods to detect, characterize, and remove motion artifact in resting state fMRI. Neuroimage 84, 320–341. doi:10.1016/j.neuroimage.2013.08.048.

Que, L., Winterer, J., Földy, C., 2019. Deep Survey of GABAergic interneurons: emerging insights from gene-isoform transcriptomics. Front. Molecul. Neurosci. 12. https://www.frontiersin.org/article/10.3389/fnmol.2019.00115.

Rubinov, M., Sporns, O., 2010. Complex network measures of brain connectivity: uses and interpretations. Neuroimage 52 (3), 1059–1069. doi:10.1016/j.neuroimage.2009.10.003.

Samuels, E., Szabadi, E., 2008. Functional neuroanatomy of the noradrenergic locus coeruleus: its roles in the regulation of arousal and autonomic function part II: physiological and pharmacological manipulations and pathological alterations of locus coeruleus activity in humans. Curr. Neuropharmacol. 6 (3), 254–285. doi:10.2174/157015908785777193.

Sara, S.J., Bouret, S., 2012. Orienting and reorienting: the locus coeruleus mediates cognition through arousal. Neuron 76 (1), 130–141. doi:10.1016/j.neuron.2012.09.011.

Schilling, K.G., Rheault, F., Petit, L., Hansen, C.B., Nath, V., Yeh, F.-C., Girard, G., Barakovic, M., Rafael-Patino, J., Yu, T., Fischi-Gomez, E., Pizzolato, M., Ocampo-Pineda, M., Schiavi, S., Canales-Rodríguez, E.J., Daducci, A., Granziera, C., Innocenti, G., Thiran, J.-P., Descoteaux, M., 2021. Tractography dissection variability: what happens when 42 groups dissect 14 white matter bundles on the same dataset? Neuroimage 243, 118502. doi:10.1016/j.neuroimage.2021.118502.

Schmitz, T.W., Duncan, J., 2018. Normalization and the cholinergic microcircuit: a unified basis for attention. Trend. Cogn. Sci. 22 (5), 422–437. doi:10.1016/j.tics.2018.02.011.

Schwarz, L.A., Luo, L., 2015. Organization of the locus coeruleus-norepinephrine system. Curr. Biol. 25 (21), R1051–R1056. doi:10.1016/j.cub.2015.09.039.

Seguin, C., Tian, Y., Zalesky, A., 2020. Network communication models improve the behavioral and functional predictive utility of the human structural connectome. Netw. Neurosci. 4 (4), 980–1006. doi:10.1162/netn_a_00161.

Shen, K., Hutchison, R.M., Bezgin, G., Everling, S., McIntosh, A.R., 2015. Network structure shapes spontaneous functional connectivity dynamics. J. Neurosci. 35 (14), 5579–5588. doi:10.1523/JNEUROSCI.4903-14.2015.

Shine, J.M., 2019. Neuromodulatory influences on integration and segregation in the brain. Trend. Cogn. Sci. 23 (7), 572–583. doi:10.1016/j.tics.2019.04.002.

Shine, J.M., 2021. The thalamus integrates the macrosystems of the brain to facilitate complex, adaptive brain network dynamics. Prog. Neurobiol. 199, 101951. doi:10.1016/j.pneurobio.2020.101951.

Shine, J.M., Aburn, M.J., Breakspear, M., Poldrack, R.A., 2018. The modulation of neural gain facilitates a transition between functional segregation and integration in the brain. ELife 7, e31130. doi:10.7554/eLife.31130.

Shine, J.M., Bissett, P.G., Bell, P.T., Koyejo, O., Balsters, J.H., Gorgolewski, K.J., Moodie, C.A., Poldrack, R.A., 2016. The dynamics of functional brain networks: integrated network states during cognitive task performance. Neuron 92 (2), 544–554. doi:10.1016/j.neuron.2016.09.018.

Shine, J.M., Breakspear, M., Bell, P.T., Ehgoetz Martens, K.A., Shine, R., Koyejo, O., Sporns, O., Poldrack, R.A, 2019. Human cognition involves the dynamic integration of neural activity and neuromodulatory systems. Nat. Neurosci. 22 (2), 289–296. doi:10.1038/s41593-018-0312-0.

Shine, J.M., Koyejo, O., Bell, P.T., Gorgolewski, K.J., Gilat, M., Poldrack, R.A., 2015. Estimation of dynamic functional connectivity using Multiplication of Temporal Derivatives. Neuroimage 122, 399–407. doi:10.1016/j.neuroimage.2015.07.064.

Shine, J.M., Müller, E.J., Munn, B., Cabral, J., Moran, R.J., Breakspear, M., 2021a. Computational models link cellular mechanisms of neuromodulation to large-scale neural dynamics. Nat. Neurosci. 24 (6), 765–776. doi:10.1038/s41593-021-00824-6.

Shine, J.M., Müller, E.J., Munn, B., Cabral, J., Moran, R.J., Breakspear, M., 2021b. Computational models link cellular mechanisms of neuromodulation to large-scale neural dynamics. Nat. Neurosci. 24 (6), 765–776. doi:10.1038/s41593-021-00824-6.

Shine, J.M., Poldrack, R.A., 2018. Principles of dynamic network reconfiguration across diverse brain states. Neuroimage 180, 396–405. doi:10.1016/j.neuroimage.2017.08.010.

Shine, J.M., van den Brink, R.L., Hernaus, D., Nieuwenhuis, S., Poldrack, R.A., 2018. Catecholaminergic manipulation alters dynamic network topology across cognitive states. Netw. Neurosci. 2 (3), 381–396. doi:10.1162/netn_a_00042.

Singleton, S.P., Luppi, A.I., Carhart-Harris, R.L., Cruzat, J., Roseman, L., Deco, G., Kringelbach, M.L., Stamatakis, E.A., Kuceyeski, A., 2021. Psychedelics Flatten the brain's energy landscape: evidence from receptor-informed network control theory. [Preprint]. Neuroscience doi:10.1101/2021.05.14.444193.

Smiley, J.F., Subramanian, M., Mesulam, M.M., 1999. Monoaminergic-cholinergic interactions in the primate basal forebrain. Neuroscience 93 (3), 817–829. doi:10.1016/s0306-4522(99)00116-5.

Smith, R.E., Tournier, J.-D., Calamante, F., Connelly, A., 2012. Anatomically-constrained tractography: improved diffusion MRI streamlines tractography through effective use of anatomical information. Neuroimage 62 (3), 1924–1938. doi:10.1016/j.neuroimage.2012.06.005.

Smith, R.E., Tournier, J.-D., Calamante, F., Connelly, A., 2015a. The effects of SIFT on the reproducibility and biological accuracy of the structural connectome. Neuroimage 104, 253–265. doi:10.1016/j.neuroimage.2014.10.004.

Smith, R.E., Tournier, J.-D., Calamante, F., Connelly, A., 2015b. SIFT2: Enabling dense quantitative assessment of brain white matter connectivity using streamlines tractography. Neuroimage 119, 338–351. doi:10.1016/j.neuroimage.2015.06.092.

Smith, S.M., 2002. Fast robust automated brain extraction. Hum. Brain Mapp. 17 (3), 143–155. doi:10.1002/hbm.10062.

Smith, S.M., Jenkinson, M., Woolrich, M.W., Beckmann, C.F., Behrens, T.E.J., Johansen-Berg, H., Bannister, P.R., De Luca, M., Drobnjak, I., Flitney, D.E., Niazy, R.K., Saunders, J., Vickers, J., Zhang, Y., De Stefano, N., Brady, J.M., Matthews, P.M., 2004. Advances in functional and structural MR image analysis and implementation as FSL. Neuroimage 23 (Suppl 1), S208–S219. doi:10.1016/j.neuroimage.2004.07.051.

Solders, S.K., Galinsky, V.L., Clark, A.L., Sorg, S.F., Weigand, A.J., Bondi, M.W., Frank, L.R., 2022. Diffusion MRI tractography of the locus coeruleus-transentorhinal cortex connections using GO-ESP. Magn. Reson. Med. 87 (4), 1816–1831. doi:10.1002/mrm.29088.

Sotiropoulos, S.N., Moeller, S., Jbabdi, S., Xu, J., Andersson, J.L., Auerbach, E.J., Yacoub, E., Feinberg, D., Setsompop, K., Wald, L.L., Behrens, T.E.J., Ugurbil, K., Lenglet, C., 2013. Effects of image reconstruction on fiber orientation mapping from multichannel diffusion MRI: Reducing the noise floor using SENSE. Magn. Reson. Med. 70 (6), 1682–1689. doi:10.1002/mrm.24623.

Sporns, O., 2013. Network attributes for segregation and integration in the human brain. Curr. Opin. Neurobiol. 23 (2), 162–171. doi:10.1016/j.conb.2012.11.015.

Suárez, L.E., Markello, R.D., Betzel, R.F., Misic, B., 2020. Linking structure and function in macroscale brain networks. Trend. Cogn. Sci. 24 (4), 302–315. doi:10.1016/j.tics.2020.01.008.

Sun, W., Tang, Y., Qiao, Y., Ge, X., Mather, M., Ringman, J.M., Shi, Y., 2020. A probabilistic atlas of locus coeruleus pathways to transentorhinal cortex for connectome imaging in Alzheimer's disease. Neuroimage 223, 117301. doi:10.1016/j.neuroimage.2020.117301.

Tagliazucchi, E., Roseman, L., Kaelen, M., Orban, C., Muthukumaraswamy, S.D., Murphy, K., Laufs, H., Leech, R., McGonigle, J., Crossley, N., Bullmore, E., Williams, T., Bolstridge, M., Feilding, A., Nutt, D.J., Carhart-Harris, R., 2016. Increased global functional connectivity correlates with LSD-induced ego dissolution. Curr. Biol. 26 (8), 1043–1050. doi:10.1016/j.cub.2016.02.010.

Teles-Grilo Ruivo, L.M., Baker, K.L., Conway, M.W., Kinsley, P.J., Gilmour, G., Phillips, K.G., Isaac, J.T.R., Lowry, J.P., Mellor, J.R., 2017. Coordinated acetylcholine release in prefrontal cortex and hippocampus is associated with arousal and reward on distinct timescales. Cell Rep. 18 (4), 905–917. doi:10.1016/j.celrep.2016.12.085.

Thiele, A., Bellgrove, M.A., 2018. Neuromodulation of attention. Neuron 97 (4), 769–785. doi:10.1016/j.neuron.2018.01.008.

Tournier, J.-D., Calamante, F., Connelly, A., 2007. Robust determination of the fibre orientation distribution in diffusion MRI: Non-negativity constrained super-resolved spherical deconvolution. Neuroimage 35 (4), 1459–1472. doi:10.1016/j.neuroimage.2007.02.016.

Tournier, J.-D., Calamante, F., Connelly, A., 2010. Improved probabilistic streamlines tractography by 2nd order integration over fibre orientation distributions. ISMRM 1.

Tournier, J.-D., Calamante, F., Connelly, A., 2012. MRtrix: diffusion tractography in crossing fiber regions. Int. J. Imaging Syst. Technol. 22 (1), 53–66. doi:10.1002/ima.22005.

Tournier, J.-D., Calamante, F., Gadian, D.G., Connelly, A., 2004. Direct estimation of the fiber orientation density function from diffusion-weighted MRI data using spherical deconvolution. Neuroimage 23 (3), 1176–1185. doi:10.1016/j.neuroimage.2004.07.037.

Tournier, J.-D., Smith, R., Raffelt, D., Tabbara, R., Dhollander, T., Pietsch, M., Christiaens, D., Jeurissen, B., Yeh, C.-H., Connelly, A., 2019. MRtrix3: A fast, flexible and open software framework for medical image processing and visualisation. Neuroimage 202, 116137. doi:10.1016/j.neuroimage.2019.116137.

Tustison, N.J., Avants, B.B., 2013. Explicit B-spline regularization in diffeomorphic image registration. Front. Neuroinformat. 7, 39. doi:10.3389/fninf.2013.00039.

Tustison, N.J., Avants, B.B., Cook, P.A., Zheng, Yuanjie, Egan, A., Yushkevich, P.A., Gee, J.C, 2010. N4ITK: improved N3 bias correction. IEEE Trans. Med. Imaging 29 (6), 1310–1320. doi:10.1109/TMI.2010.2046908.

Uddin, L.Q., 2013. Complex relationships between structural and functional brain connectivity. Trends Cogn. Sci. 17 (12), 600–602. doi:10.1016/j.tics.2013.09.011.

Van Essen, D.C., Smith, S.M., Barch, D.M., Behrens, T.E.J., Yacoub, E., Ugurbil, K., 2013. The WU-minn human connectome project: an overview. Neuroimage 80, 62–79. doi:10.1016/j.neuroimage.2013.05.041.

Wainstein, G., Müller, E.J., Taylor, N.L., Munn, B.R., Shine, J.M., 2022. A bow to the brain's violin: the role of the locus coeruleus in shaping adaptive cortical melodies. Trend. Cogn. Sci..

Wainstein, G., Rojas-Líbano, D., Medel, V., Alnæs, D., Kolskår, K.K., Endestad, T., Laeng, B., Ossandon, T., Crossley, N., Matar, E., Shine, J.M., 2021. The ascending arousal system promotes optimal performance through mesoscale network integration in a visuospatial attentional task. Netw. Neurosci. 1–21. doi:10.1162/netn_a_00205.

Watanabe, T., 2021. Causal roles of prefrontal cortex during spontaneous perceptual switching are determined by brain state dynamics. ELife 10, e69079. doi:10.7554/eLife.69079.

Watanabe, T., Masuda, N., Megumi, F., Kanai, R., Rees, G., 2014. Energy landscape and dynamics of brain activity during human bistable perception. Nat. Commun. 5 (1), 4765. doi:10.1038/ncomms5765.

Ye, R., Rua, C., O'Callaghan, C., Jones, P.S., Hezemans, F.H., Kaalund, S.S., Tsvetanov, K.A., Rodgers, C.T., Williams, G., Passamonti, L., Rowe, J.B., 2021. An in vivo probabilistic atlas of the human locus coeruleus at ultra-high field. Neuroimage 225, 117487. doi:10.1016/j.neuroimage.2020.117487.

Zaborszky, L., Csordas, A., Mosca, K., Kim, J., Gielow, M.R., Vadasz, C., Nadasdy, Z., 2015. Neurons in the Basal Forebrain Project to the cortex in a complex topographic organization that reflects corticocortical connectivity patterns: an experimental study based on retrograde tracing and 3D reconstruction. Cereb. Cortex 25 (1), 118–137. doi:10.1093/cercor/bht210.

Zaborszky, L., Cullinan, W.E., Luine, V.N., 1993. Chapter 3: catecholaminergic-cholinergic interaction in the basal forebrain. In: Progress in Brain Research, 98. Elsevier, pp. 31–49. doi:10.1016/S0079-6123(08)62379-1.

Zaborszky, L., Gombkoto, P., 2017. The cholinergic multicompartmental basal forebrain microcircuit. Handbook of Brain Microcircuits. Oxford University Press.

Zaborszky, L., Hoemke, L., Mohlberg, H., Schleicher, A., Amunts, K., Zilles, K., 2008. Stereotaxic probabilistic maps of the magnocellular cell groups in human basal forebrain. Neuroimage 42 (3), 1127–1141. doi:10.1016/j.neuroimage.2008.05.055.

Zhang, Y., Brady, M., Smith, S., 2001. Segmentation of brain MR images through a hidden Markov random field model and the expectation-maximization algorithm. IEEE Trans. Med. Imaging 20 (1), 45–57. doi:10.1109/42.906424.

Zimmermann, J., Ritter, P., Shen, K., Rothmeier, S., Schirner, M., McIntosh, A.R., 2016. Structural architecture supports functional organization in the human aging brain at a regionwise and network level: structure supports function in aging. Hum. Brain Mapp. 37 (7), 2645–2661. doi:10.1002/hbm.23200.